Normal-state magnetotransport properties of -FeSe superconductors



2016 EPL 113 17005

(http://iopscience.iop.org/0295-5075/113/1/17005)

A Letters Journal Exploring the Frontiers of Physics

January 2016

EPL, **113** (2016) 17005
doi: 10.1209/0295-5075/113/17005

www.epljournal.org

# Normal-state magnetotransport properties of $\beta$-FeSe superconductors

J. D. Querales-Flores[1,2], M. L. Amigó[1,2], G. Nieva[1,2] and C. I. Ventura[1,3]

[1] *Centro Atómico Bariloche-CNEA and CONICET - Av. Bustillo 9500, 8400 Bariloche, Argentina*
[2] *Instituto Balseiro, Universidad Nacional de Cuyo and CNEA - 8400 Bariloche, Argentina*
[3] *Sede Andina, Universidad Nacional de Río Negro - 8400 Bariloche, Argentina*

received 19 November 2015; accepted 6 January 2016
published online 28 January 2016

PACS 74.25.F- – Transport properties
PACS 74.70.Xa – Pnictides and chalcogenides
PACS 71.10.-w – Theories and models of many-electron systems

**Abstract** – We present $\beta$-FeSe magnetotransport data, and describe them theoretically. Using a simplified microscopic model with two correlated effective orbitals, we determined the normal state electrical conductivity and Hall coefficient, using Kubo formalism. With model parameters relevant for Fe-chalcogenides, we describe the observed effect of the structural transition on the *ab*-plane electrical resistivity, as well as on the magnetoresistance. Temperature-dependent Hall coefficient data were measured at 16 tesla, and their theoretical description improves upon inclusion of moderate electron correlations. We confirm the effect of the structural transition on the electronic structure, finding deformation-induced band splittings comparable to those reported in angle-resolved photoemission.



**Introduction.** – Since the discovery of superconductivity in $LaFeAsO_{1-x}F_x$ [1], several types of iron-based superconductors have been reported. The so-called "11" family of FeSe superconductors attracted much attention due to their simpler crystal structure, and particular electronic and physical properties. Since the first report of superconductivity with critical temperature $T_c = 8\,\mathrm{K}$ for PbO-type $\alpha$-$FeSe_{0.88}$ by Hsu *et al.* [2], a $T_c$ of 37 K at a pressure of 8.9 GPa was already reached [3]. FeSe compounds have a band structure similar to that of ferropnictides [4,5]. $FeSe_{1-x}$ with Se deficiency was reported to exhibit anomalies related to spin density waves (SDW) and magnetic ordering at temperatures near 100 K [6]. On the other hand, ref. [7] reported that FeSe exhibited superconductivity within a narrow range of stoichiometries, $Fe_{1.01\pm0.02}Se$, without magnetic ordering.

Pure $\beta$-FeSe undergoes a structural transition from a low-temperature orthorhombic to a tetragonal phase at $T_s \sim 90\,\mathrm{K}$, not accompanied by a SDW, and the compound exhibits superconductivity below $T_c = 8.87\,\mathrm{K}$. Angle-resolved photoemission spectroscopy (ARPES) experiments in $\beta$-FeSe revealed a significant change in the electronic structure when going through the structural transition [8]. Recently it was claimed [9] that the observed changes in electronic structure could not be explained by the small lattice distortion, an issue which we will address in our present work.

Recently, Amigó *et al.* [10] reported that multiband effects are needed to describe the magnetotransport properties of $\beta$-FeSe ($Fe_{0.96}Se$) single crystals. Concretely, in the normal state below 90 K, a strongly anisotropic positive magnetoresistance, that becomes negligible above that temperature, was found. This magnetoresistance and the upper critical field could be understood with a phenomenological uncorrelated two-band model. Also a recent ultra-high magnetic-field study [11] reported that magnetotransport in FeSe results from a small multiband Fermi surface (FS) with different carrier mobilities.

In this work, to study normal-state magnetotransport properties of $\beta$-FeSe superconductors, we propose to employ a minimal microscopic model, which includes two effective bands describing the low-energy electronic structure, as well as intra- and inter-orbital Coulomb interactions. Previously [12] we treated the model using perturbative techniques to determine the electron Green's functions and the temperature-dependent spectral density function. The kinetic energy part of the Hamiltonian is represented by the effective two-orbital model proposed by Raghu *et al.* in ref. [13], consisting of a two-dimensional lattice for the Fe atoms, with two degenerate orbitals

per site. Tight-binding parameters were fitted to obtain an effective band structure describing the Fermi surface topology of ferropnictides [13,14]. The two-orbital model was shown to be suitable to describe the extended $s$-wave pairing and other superconducting properties of these systems [14–21].

**Calculation of magnetotransport properties of FeSe compounds.** –

*Microscopic two-orbital minimal model for FeSe.* To describe analytically the normal-state magnetotransport properties of FeSe superconductors, we will consider the following minimal model preserving the essential low-energy physics:

$$\mathcal{H} = \mathcal{H}_0 + V_{int}. \tag{1}$$

The kinetic energy part of the Hamiltonian in eq. (1) is given by the uncorrelated two-orbital model by Raghu *et al.* [13] mentioned in the Introduction:

$$\mathcal{H}_0 = \sum_{k,\sigma} \Big[ E_c(k) c^\dagger_{k\sigma} c_{k\sigma} + E_d(k) d^\dagger_{k\sigma} d_{k\sigma} \Big], \tag{2}$$

where $c^\dagger_{k\sigma}$ creates an electron with crystal momentum $\vec{k}$ and spin $\sigma$ in the effective band with energy $E_c(\vec{k})$, likewise for $d^\dagger_{k\sigma}$ and $E_d(\vec{k})$. The effective band energies are

$$E_{\substack{d\\c}}(\vec{k}) = \epsilon_+(\vec{k}) \pm \sqrt{\epsilon^2_-(\vec{k}) + \epsilon^2_{xy}(\vec{k})} - \mu, \tag{3}$$

where $\mu$ denotes the chemical potential at temperature $T$, and

$$\begin{aligned}
\epsilon_\pm(\vec{k}) &= \frac{\epsilon_x(\vec{k}) \pm \epsilon_y(\vec{k})}{2}; \quad \epsilon_{xy}(\vec{k}) = -4t_4 \sin(k_x)\sin(k_y),\\
\epsilon_x(\vec{k}) &= -2t_1\cos(k_x) - 2t_2\cos(k_y) - 4t_3\cos(k_x)\cos(k_y),\\
\epsilon_y(\vec{k}) &= -2t_2\cos(k_x) - 2t_1\cos(k_y) - 4t_3\cos(k_x)\cos(k_y).
\end{aligned}$$

The tight-binding parameters $t_i, i = 1-4$, denote the hopping amplitudes between sites of the two-dimensional lattice of Fe atoms, derived in ref. [13] as $t_1 = -1\,\text{eV}$, $t_2 = 1.3\,\text{eV}$ , $t_3 = t_4 = -0.85\,\text{eV}$.

The electron correlations are represented by $V_{int}$ in eq. (1). The effect of local intra- and inter-orbital correlations in ferropnictides was previously studied [12,19,22]. It was found that the inter-orbital correlation was less relevant than the intra-orbital one. Therefore, in our minimal model for FeSe we consider only the local intra-orbital Coulomb repulsion $U$:

$$V_{int} = \sum_i U(n_{i\uparrow}n_{i\downarrow} + N_{i\uparrow}N_{i\downarrow}), \tag{4}$$

where $n_{i\sigma} = c^\dagger_{i\sigma}c_{i\sigma}$ and $N_{i\sigma} = d^\dagger_{i\sigma}d_{i\sigma}$, and $i$ denotes the Fe-lattice sites. Since correlations in FeSe compounds are intermediate [12,23–27], and mainly motivated by the fact that it had been possible to describe previous magnetotransport results in terms of a phenomenological model with two uncorrelated carrier bands [10], here we decided to use Hartree-Fock approximation (HF) for the correlations. A recent study of the effect of correlations in FeSe [27], which found no relevant qualitative differences employing density functional theory (DFT) calculations and DFT + DMFT (DFT with dynamical mean-field theory) for the FS and the low-energy spectral properties, provides further justification for the level of approximation we used. We determined the HF renormalized band structure, and self-consistently calculated $\mu(T)$ for total electron filling $n$ of the two renormalized effective bands (see ref. [12] for details).

*Calculation of the electrical conductivity tensor and Hall coefficient.* To describe magnetotransport in FeSe compounds, we evaluated the electrical conductivity tensor $\sigma_{\alpha\beta}$, defined by

$$\langle j_\alpha(t)\rangle = \sigma_{\alpha\beta}E_\beta(t), \tag{5}$$

where $\langle j_\alpha(t)\rangle$ is the average current at temperature $T$ and time $t$ flowing in the $\alpha$-direction, in response to an electric field, $E_\beta(t)$, applied in the $\beta$-direction.

Assuming the presence of a magnetic field $\vec{H} = H_z\hat{z}$ perpendicular to the $ab$-plane of FeSe, and the electric current flowing in the $x$-direction ($j_x$) as a result of an electric field along $\hat{x}$ plus the Hall electric field along $\hat{y}$ we have

$$\langle j_x\rangle = \sigma_{xx}(\omega)E_x(t) + \sigma_{xy}(\omega)E_y(t), \tag{6}$$

where $\sigma_{xx}(\omega)$ and $\sigma_{xy}(\omega)$ are, respectively, the longitudinal and transversal components of the electrical conductivity tensor. To compare our analytical results with experiments, we determined the $ab$-plane dc-resistivity ($\rho_{xx}$) and the Hall resistivity ($\rho_{xy}$) as the static (zero-frequency, *i.e.* $\omega \to 0$) limit of

$$\rho_{xx} = \frac{\sigma_{xx}(\omega)}{\sigma^2_{xx}(\omega) + \sigma^2_{xy}(\omega)}; \quad \rho_{xy} = \frac{\sigma_{xy}(\omega)}{\sigma^2_{xx}(\omega) + \sigma^2_{xy}(\omega)}. \tag{7}$$

In the Kubo formulation for transport [28,29], $\sigma_{\alpha\beta}$ are given by appropriate generalised susceptibilities $\chi_{AB}(\omega)$, measuring the linear response of observable $A$ of a system to an applied external field coupling to its observable $B$. The susceptibilities, in turn, can be calculated using retarded Green's functions, $\langle\langle A; B\rangle\rangle(\omega)$ [29,30]. Here

$$\sigma_{xx}(\omega) = \chi_{j_x,eX}(\omega) = \langle\langle j_x; eX\rangle\rangle(\omega), \tag{8}$$

$$\sigma_{xy}(\omega) = \chi_{j_x,eY}(\omega) = \langle\langle j_x; eY\rangle\rangle(\omega), \tag{9}$$

where $X$ and $Y$ are the respective components of the system's position operator. The electron Green's functions include a sum of the respective contributions from the $c$ and $d$ effective bands, which can each be calculated from the following exact set of equations of motion (EOM) [30]:

$$\begin{aligned}
\omega\langle\langle j_x, eX\rangle\rangle^{c,d} &= \frac{1}{2\pi}\langle[j^{c,d}_x, eX]\rangle + \langle\langle[j^{c,d}_x, \mathcal{H}]; eX\rangle\rangle,\\
\omega\langle\langle j_x, eY\rangle\rangle^{c,d} &= \frac{1}{2\pi}\langle[j^{c,d}_x, eY]\rangle + \langle\langle[j^{c,d}_x, \mathcal{H}]; eY\rangle\rangle,
\end{aligned} \tag{10}$$

where the current operator [31] is defined as $j_x^c = \frac{e}{m_c^*}\sum_{\vec{k},\sigma} k_x c^\dagger_{\vec{k},\sigma} c_{\vec{k},\sigma}$ and $j_x^d = \frac{e}{m_d^*}\sum_{\vec{k},\sigma} k_x d^\dagger_{\vec{k},\sigma} d_{\vec{k},\sigma}$, being $m_i^*$, $i = c, d$, the effective masses of the carriers in each band. New higher-order Green's functions appear coupled in eqs. (10). In order to close the system of coupled equations of motion we used HF approximation to decouple them, and determined $\langle\langle j_x, eX\rangle\rangle$ and $\langle\langle j_x, eY\rangle\rangle$ in first order of perturbations on the electron correlation $U$. The final expressions obtained for the $ab$-plane electrical conductivity components, in the presence of $\vec{H} = H_z\hat{z}$, read

$$\sigma_{xx}(\omega) = \frac{e^2}{\Omega}\sum_{\vec{k},\sigma}\left\{\frac{\langle c^\dagger_{\vec{k}\sigma} c_{\vec{k}\sigma}\rangle}{\hbar(\omega-\omega_c) - n_c E_c(\vec{k}) - 2Un_c^2} + \frac{\langle d^\dagger_{\vec{k}\sigma} d_{\vec{k}\sigma}\rangle}{\hbar(\omega-\omega_d) - n_d E_d(\vec{k}) - 2Un_d^2}\right\}, \quad (11)$$

$$\sigma_{xy}(\omega) = \frac{ne}{H_z} + \frac{e^2}{\Omega}\sum_{\vec{k},\sigma}\phi(\vec{k})\left\{\frac{1}{\hbar\omega - \tilde{E}_c(\vec{k}) + \hbar(\omega+\omega_c)} - \frac{1}{-\hbar\omega - \tilde{E}_c(\vec{k}) + \hbar(\omega-\omega_c)} + \frac{1}{\hbar\omega - \tilde{E}_d(\vec{k}) + \hbar(\omega+\omega_d)} - \frac{1}{-\hbar\omega - \tilde{E}_d(\vec{k}) + \hbar(\omega-\omega_d)}\right\}, \quad (12)$$

where $\Omega$ is the unit cell volume, $\tilde{E}_i(\vec{k}) = E_i(\vec{k}) + 2Un_i^2$ for $i = c, d$. Above: $\phi(\vec{k}) \equiv (\frac{\langle c^\dagger_{\vec{k}\sigma} c_{\vec{k}\sigma}\rangle - \langle d^\dagger_{\vec{k}\sigma} d_{\vec{k}\sigma}\rangle}{E_d(\vec{k}) - E_c(\vec{k})})$, being $\omega_i \equiv \frac{eH_z}{c}(\frac{1}{m_i^*})$ $(i = c, d)$, *i.e.* the cyclotron frequency of $c$ and $d$ electrons. $m_i^*$, $i = c, d$ represent the diagonal components of the effective mass tensor, given by $(\frac{1}{m_i^*})_{\mu\nu} = \frac{1}{\hbar^2}\frac{\partial^2 E_i(\vec{k})}{\partial k_\mu \partial k_\nu}$. The conductivity due to multiple band maxima or minima is proportional to the sum of the inverse of the individual masses, multiplied by the density of carriers in each band, to take into account all contributions to the conductivity [32]. To evaluate the conductivities, we used the Chadi-Cohen BZ sampling method [33,34] for square and rectangular lattices, to perform the required BZ summations.

The following expression for the Hall coefficient ($R_H$) was obtained, using eq. (12):

$$R_H = \frac{1}{\sigma_{xy} H_z}; \quad \sigma_{xy} = \lim_{\substack{\omega\to 0\\ \delta\to 0^+}} \Re\left[\sigma_{xy}(\omega + i\delta)\right] \equiv \left(\frac{1}{\gamma_c + \gamma_d}\right),$$
$$\gamma_i \equiv \left\{\left(\frac{en_i}{m_i^*}\right)\frac{(\omega+\omega_i)\left[(\omega-\omega_i)^2+\delta^2\right] + (\omega-\omega_i)\left[(\omega+\omega_i)^2+\delta^2\right]}{(\omega+\omega_i)^2(\omega-\omega_i)^2 + \delta^2(\omega+\omega_i)^2 - \delta^2(\omega-\omega_i)^2 + \delta^4}\right\}. \quad (13)$$

In the next section, we will compare our Hall coefficient results with those obtained using the classical expression for two types of uncorrelated carriers (with charge $e$): [35]

$$R_H = \frac{1}{e}\frac{(\mu_c^2 n_c + \mu_d^2 n_d) + (\mu_c\mu_d H_z)^2(n_c + n_d)}{(\mu_c n_c + \mu_d n_d)^2 + (\mu_c\mu_d H_z)^2(n_c + n_d)^2}, \quad (14)$$

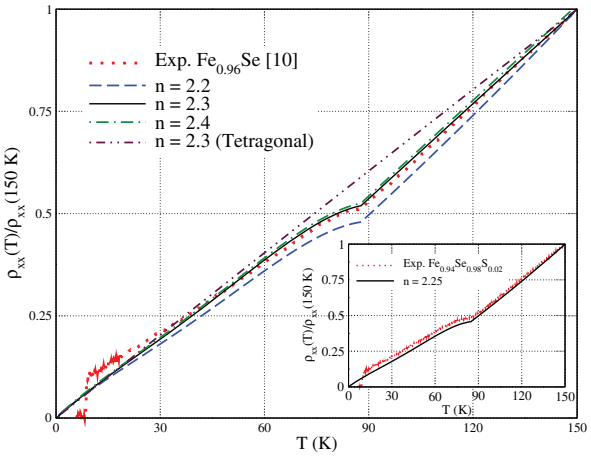


Fig. 1: (Colour online) $H = 0$: $ab$-plane resistivity as a function temperature. $\rho_{xx}(T)/\rho_{xx}(150\,\mathrm{K})$, calculated for different doping values (indicated in the figure): using the temperature-dependent lattice parameters, $a(T)$ and $b(T)$, reported for FeSe [37]. Also included is the result obtained assuming a tetragonal lattice, with constant lattice parameter: $a = b = 3.77\,\text{Å}$ (double-dot–dashed line). Experimental curve (dotted line): $Fe_{0.96}Se$ single crystal, from ref. [10]. Inset: experimental $\rho_{xx}(T)/\rho_{xx}(150\,\mathrm{K})$ (dotted line) measured for a $Fe_{0.94}Se_{0.98}S_{0.02}$ single crystal, and calculated curve (solid line) for $n = 2.25$. Model parameters used: $U = 3$, $t_1 = -1.0$, $t_2 = 1.3$, $t_3 = t_4 = -0.85$. All energies are in eV. Chadi-Cohen [33,34] order for BZ summations: $\nu = 9$.

where $\mu_i$, $i = c, d$, denotes the mobility in each electron band. One has $\mu_i = e\tau_i/m_i^* = \sigma_i/(en_i)$ [36], being $\tau_i^{-1}$ and $\sigma_i$, respectively, the scattering rates and dc-conductivities for the electrons in each band.

**Results and discussion.** – We present magnetotransport results for the normal state of FeSe compounds, and compare them with those calculated as presented in the previous section. Using the optimal correlation value $U = 3\,\mathrm{eV}$, previously found to describe best other electronic properties of these compounds [12], we analize the dependence on temperature, doping and magnetic field $H_z = H$, and compare our results with new experimental data and those of ref. [10], as well as with the results obtained assuming uncorrelated electrons. Notice that the value $U = 3\,\mathrm{eV}$ represents less than one-third, $\sim 0.29$, of the total bandwidth for uncorrelated electrons [13], thus characterising FeSe compounds as systems with intermediate electron correlations as discussed in the previous section.

First, in fig. 1 we study the temperature dependence of the $ab$-plane dc-resistivity, represented by $\rho_{xx}(T)$, for $Fe_{0.96}Se$ and $Fe_{0.94}Se_{0.98}S_{0.02}$ single crystals in the absence of magnetic field, measured with a standard 4-points dc-technique. The main figure compares the experimental data (normalized at $T = 150\,\mathrm{K}$) with two calculations using our approach: one for a tetragonal crystal with constant lattice parameters (the normalized resistivity

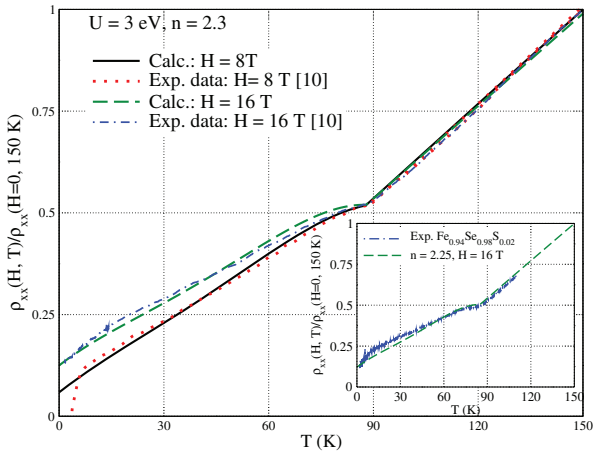


Fig. 2: (Colour online) Effect of a magnetic field parallel to the $c$-axis: temperature dependence of the $ab$-plane resistivity (normalized to $\rho(150\,\mathrm{K}, H = 0)$) for $Fe_{0.96}Se$ ($n = 2.3$) in the main figure. Calculated and experimental [10] results for $H = 8\,\mathrm{T}$, $16\,\mathrm{T}$, as indicated in the plot. Other parameters as in fig. 1. Inset: calculated and experimental [10] $ab$-plane resistivity (normalized to $\rho(150\,\mathrm{K}, H = 0)$) of $Fe_{0.94}Se_{0.98}S_{0.02}$ for $H = 16\,\mathrm{T}$.

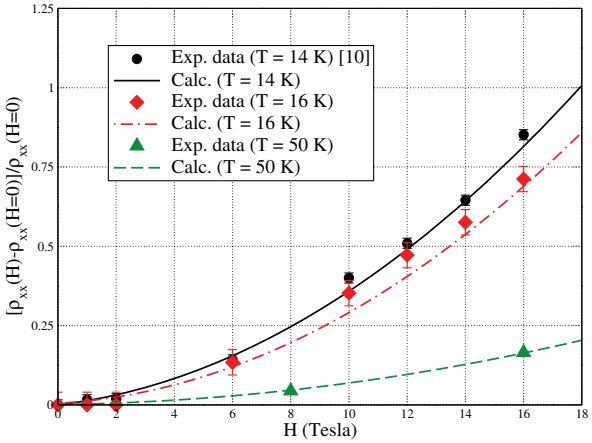


Fig. 3: (Colour online) Magnetoresistance as a function of $H$ parallel to the $c$-axis: calculated (lines) and experimental (symbols) results for temperatures $T = 14$, 16, and $50\,\mathrm{K}$, as indicated in the plot. The experimental data at $T = 14\,\mathrm{K}$ are taken from ref. [10]. Model parameters: $U = 3\,\mathrm{eV}$, $n = 2.3$ and others as in fig. 1.

plotted has negligible dependence on doping up to 150 K), while the other, more realistic, takes into account the $T$-dependence of the lattice parameters $a(T), b(T)$ of FeSe [37] and, in particular, the structural transition [10,38], which occurs at $T_s \sim 90\,\mathrm{K}$ for the $Fe_{0.96}Se$ sample, and at 87 K for the $Fe_{0.94}Se_{0.98}S_{0.02}$ one. As expected, a clear improvement of the description of the $ab$-plane dc-resistivity at $H = 0$ is obtained using the $T$-dependent lattice parameters of FeSe [37]. The best agreement to the experimental data is obtained considering a total electron filling $n = 2.3$ (main figure), and 2.25 (inset), for the correlated two-orbital model, which corresponds to an Fe-content of $x = 0.96$, and $x = 0.94$, respectively. In accordance with experiment, the calculated $ab$-plane resistivity presents a metallic-like behavior in the normal state with a change of slope around the structural transition temperature. Hence, we will continue using the temperature-dependent lattice parameters in what follows.

In the next three figures we will present magnetotransport results obtained under applied magnetic fields parallel to the $c$-axis of the $Fe_xSe$ samples: *i.e.* perpendicular to the plane formed by the Fe atoms.

In fig. 2, the main figure exhibits the normal-state $ab$-plane resistivity $\rho_{xx}(T)$ calculated and measured at magnetic fields of 8 T and 16 T, having fixed the total band filling at $n = 2.3$ to describe $Fe_{0.96}Se$. In the inset we show $\rho_{xx}(T)$ at 16 tesla for the $Fe_{0.94}Se_{0.98}S_{0.02}$ sample, with the corresponding calculated curve using $n = 2.25$. Notice that above $T_c = 8.87\,\mathrm{K}$ for $Fe_{0.96}Se$ [10], and above $T_c = 10.06\,\mathrm{K}$ for $Fe_{0.94}Se_{0.98}S_{0.02}$, we obtain very good agreement. A change of slope of the resistivity at the structural transition temperature is seen, and, in particular, our results describe the positive magnetoresistance observed below $T_s$ [10] and the negligible one above $T_s$.

In fig. 3 we present calculated and experimental magnetoresistance results for $Fe_{0.96}Se$ as a function of the magnetic field parallel to $c$, at three different temperatures. Only the experimental $T = 14\,\mathrm{K}$ results included have been published before [10]. Notice the remarkable agreement at $T = 14\,\mathrm{K}$, 16 K, and 50 K between the experimental magnetoresistance and the values calculated assuming $U = 3\,\mathrm{eV}$ and $n = 2.3$. In particular, our results describe a quadratic $\sim H^2$ behavior of the magnetoresistance, consistently with the prediction from a phenomelogical two-band model used in ref. [10]. In the present work, we also find experimentally and describe theoretically that the magnetoresistance concavity (and therefore also its magnitude) is monotonically reduced as temperature is increased towards $T_s \sim 90\,\mathrm{K}$, which is consistent with the results in fig. 2, and in agreement with recent measurements included in an ultra-high magnetic field study of FeSe [11].

At $T = 40\,\mathrm{K}$, we find effective masses: $m_c^* = 2.63 m_e$ and $m_d^* = 3.46 m_e$, in agreement with DFT + DMFT calculations by Aichhorn *et al.* [23], where a significant orbital-dependent mass renormalization in the range 2–5 was predicted, and confirmed by ARPES results at $T = 40\,\mathrm{K}$ [24].

Next, in fig. 4, we present experimental and theoretical results obtained for the Hall coefficient $R_H$ in a $Fe_{0.94}Se_{0.98}S_{0.02}$ single crystal as a function of temperature, at $H = 16\,\mathrm{T}$ parallel to the $c$-axis. The Hall contribution was measured with a standard dc-technique using four contacts along two perpendicular lines, separating the small resistivity contributions by measuring in positive and negative magnetic fields along the $c$-axis. We also included in fig. 4 the theoretical result obtained with our analytical approach, for the correlated two-orbital model

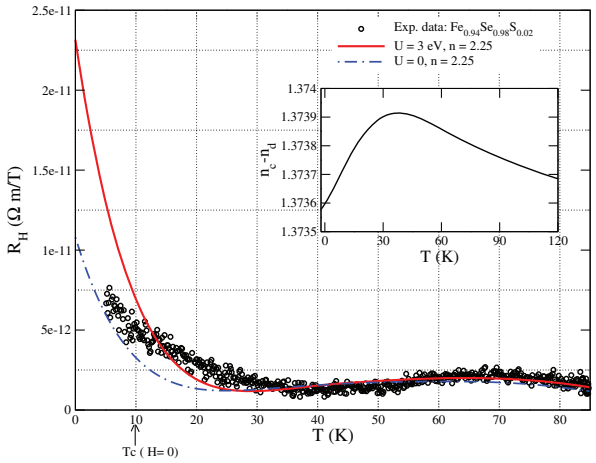


Fig. 4: (Colour online) Temperature dependence of the Hall coefficient at $H = 16\,\mathrm{T}$. Comparison between: our experimental results for $Fe_{0.94}Se_{0.98}S_{0.02}$ (points), and two theoretical calculations: present analytical approach (solid line) for the correlated two-orbital model ($U = 3\,\mathrm{eV}$, $n = 2.25$, other parameters as in fig. 1), and phenomenological uncorrelated two-carrier model: eq. (14) (dot-dashed line). An arrow indicates the critical temperature of the sample at $H = 0$. The inset shows the effect of temperature on the difference $(n_c - n_d)$ of the partial fillings of the effective bands in our correlated two-orbital model.

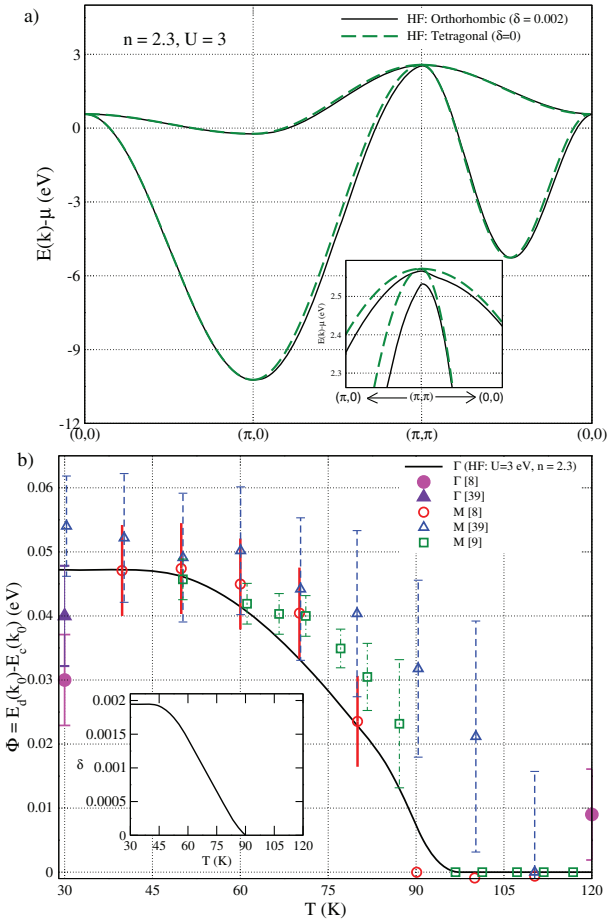


Fig. 5: (Colour online) $H = 0$, effect of lattice deformation $\delta$ on the electronic structure. (a) Band structure of the correlated two-orbital model in Hartree-Fock approximation shown in the large (unfolded) BZ [13], *i.e.* one Fe/cell, at $\delta = 0$ (dashed line) and $\delta = 0.002$ (solid line). $T = 10\,\mathrm{K}$, $n_c = 1.87$ and $n_d = 0.43$. Inset: amplification near $\vec{k}_0 = (\pi, \pi)$, which corresponds to the zone center $\Gamma$ in the small (folded) BZ, *i.e.* two Fe/cell. (b) $T$-dependence of the band splitting at two BZ points: denoted as $\Gamma$ and $M$ in the small BZ. Concretely: $T$-dependence of the calculated band splitting at $\Gamma$, and for comparison we include the respective ARPES data at $\Gamma$ and $M$. Inset: temperature dependence of the deformation parameter using the lattice parameters of ref. [37].

with parameters $U = 3\,\mathrm{eV}$ and filling $n = 2.25$. Notice the good agreement obtained with the experimental data. We found that, in our theoretical approach, $R_H$, apart from its dependence on the magnetic field, is very sensitive to total electron filling $n$, presenting qualitative sizeable changes depending on the Fe-content. These changes are related to the position of the Fermi level with respect to the effective model's band structure [12,13] (which can be seen in fig. 5(a)). The theoretical curve in fig. 4 corresponds to a multi-band situation in which the Fermi level crosses the two $c$ and $d$ correlated bands, with unequal fillings of those bands. In particular, the inset depicts the temperature dependence of the difference $(n_c - n_d)$ between the partial fillings of these bands at total filling $n = 2.25$. Notice that it is maximum at the same temperature, $\sim 38\,\mathrm{K}$, at which the dependence on temperature of the lattice parameters sets in. This maximum coincides with the inflection point in $R_H(T)$, which we checked that also occurs at $H = 16\,\mathrm{T}$ if two uncorrelated carrier bands contributed to $R_H(T)$ according to eq. (14). The latter case is also shown in fig. 4, using the carrier mobilities and densities obtained from our approach for $U = 0$ and $n = 2.25$. Figure 4 evidentiates that better agreement to the experimental data is obtained with the correlated two-orbital model, than in the absence of electron correlations.

To end, we discuss the effect of the lattice deformation related to the structural transition on the electronic properties of FeSe superconductors, in the absence of magnetic field. It has been suggested that the emergence of magnetoresistance in FeSe superconductors below $T_s$ might be related to changes in the electronic structure [8,10]. On the HF renormalized band structure of our effective correlated two-orbital model for FeSe compounds, the main effects of the deformation are found in the BZ region around $\vec{k}_0 = (\pi, \pi)$ of the large BZ, *i.e.*, with one Fe/cell [13], as fig. 5(a) shows. We include results for two values of the orthorhombicity parameter $\delta = (a - b)/(a + b)$ [8], namely, $\delta = 0$ and $\delta = 0.002$. Our results indicate that the energetically non-equivalent $xz$ and $yz$ orbitals [13] become degenerate at and above the structural transition, in agreement with recent ARPES experiments [8]. The symmetry breaking, manifested in the band splitting appearing at $\vec{k}_0$,

results from the lattice deformation from tetragonal to orthorhombic. Next, fig. 5(b) exhibits the temperature dependence we calculated for the band splitting at $\vec{k_0}$, measured by $\Phi(T) = E_d(\vec{k_0}) - E_c(\vec{k_0})$. Notice that $\vec{k_0}$ of the large BZ, corresponds to the centre of the small BZ obtained with two Fe/cell, *i.e.* $\Gamma$. For comparison, in fig. 5(b) we also include ARPES results for $\Phi(T)$ at $\Gamma$ and $M$ (using the small BZ notation, as in ARPES [8,9,39]). Reference [8] mentions that the band splitting measured at $M$ is nearly comparable to that at $\Gamma$, possibly due to the relatively large error bars for these data. The inset of fig. 5(b) depicts the $T$-dependence of $\delta$, resulting from the $T$-dependent FeSe lattice parameters of ref. [37].

**Conclusions.** – We studied magnetotransport in the normal state of $Fe_xSe$ compounds, presenting experimental data obtained in single crystals as well as a theoretical description of the results. Using a simplified microscopic model to describe the compounds, based on two correlated effective orbitals, we determined the normal-state electrical conductivity tensor and Hall coefficient in the linear response regime, employing the Kubo formulation. We decoupled the equations of motion for the current-current correlation functions in first-order (Hartree-Fock) approximation, with model parameters in the range relevant for Fe-chalcogenides, previously used to describe their spectral properties. With this simplified model we could successfully describe i) the effect of the structural transition from a tetragonal to an orthorhombic phase observed in the *ab*-plane electrical resistivity; ii) the positive magnetoresistance in the presence of a magnetic field perpendicular to the *ab*-plane in the orthorhombic phase, which becomes negligible above the structural transition temperature; iii) the Hall coefficient $R_H$ as a function of temperature, showing that the inclusion of moderate electron correlations improves the description of the experimental results; iv) effects of the lattice deformation related to the structural transition on the electronic properties of FeSe superconductors: we found changes in the electronic structure below the structural phase transition temperature, comparable to those reported in ARPES experiments.

Our work presents experimental and theoretical evidence confirming the key role of the structural transition on the strongly anisotropic magnetotransport properties observed in the normal state of $\beta$-FeSe superconductors, and that moderately correlated multiband models can provide the best description of these experimental results.

* * *

GN and CIV are researchers of CONICET (Argentina). MLA. and JDQ-F have CONICET fellowships. We acknowledge support from CONICET (PIP 0448 and PIP 0702), ANPCyT (PICT Raices'2012, No. 1069) and SeCTyP-UNCuyo.

REFERENCES

[1] Kamihara Y. *et al.*, *J. Am. Chem. Soc.*, **130** (2008) 3296.
[2] Hsu F. C. *et al.*, *Proc. Natl. Acad. Sci. U.S.A.*, **105** (2008) 14262.
[3] Medvedev S. *et al.*, *Nat. Mater.*, **8** (2009) 630.
[4] Subedi A. *et al.*, *Phys. Rev. B*, **78** (2008) 134514.
[5] Liu Xu *et al.*, *J. Phys.: Condens. Matter*, **27** (2015) 183201.
[6] Lee K. W., Pardo V. and Pickett W. E., *Phys. Rev. B*, **78** (2008) 174502.
[7] McQueen T. M. *et al.*, *Phys. Rev. B*, **79** (2009) 014522.
[8] Shimojima T. *et al.*, *Phys. Rev. B*, **90** (2014) 121111(R).
[9] Watson M. D. *et al.*, *Phys. Rev. B*, **91** (2015) 155106.
[10] Amigó M. L. *et al.*, *J. Phys.: Conf. Ser.*, **568** (2014) 022065.
[11] Watson M. D. *et al.*, *Phys. Rev. Lett.*, **115** (2015) 027006.
[12] Querales-Flores J. D., Ventura C. I., Citro R. and Rodríguez-Núñez J. J., arXiv:1502.08042v3 (2015).
[13] Raghu S. *et al.*, *Phys. Rev. B*, **77** (2008) 220503(R).
[14] Yao Zi-Jian *et al.*, *New J. Phys.*, **11** (2009) 025009.
[15] Graser S. *et al.*, *New J. Phys.*, **11** (2009) 025016.
[16] Hu Jiangping and Hao Ningning, *Phys. Rev. X*, **2** (2012) 021009.
[17] Liu Guang-Kun *et al.*, *J. Phys.: Condens. Matter*, **26** (2014) 325601.
[18] Ran Ying *et al.*, *Phys. Rev. B*, **79** (2009) 014505.
[19] Dagotto E. *et al.*, *Front. Phys.*, **6** (2011) 379.
[20] Zhou Y., Xu D., Zhang F. and Chen W., *EPL*, **95** (2011) 17003.
[21] Hu Xiang, Ting C. S. and Zhu Jian-Xin, *Phys. Rev. B*, **80** (2009) 014523.
[22] Scalapino D. J., *Rev. Mod. Phys.*, **84** (2012) 1383.
[23] Aichhorn M. *et al.*, *Phys. Rev. B*, **82** (2010) 064504.
[24] Maletz J. *et al.*, *Phys. Rev. B*, **89** (2014) 220506(R).
[25] Craco L. and Leoni S., *Mater. Res. Express*, **1** (2014) 036001.
[26] Craco L., Laad M. S. and Leoni S., *J. Phys.: Conf. Ser.*, **487** (2014) 12017.
[27] Leonov I., Skornyakov S. L., Anisimov V. I. and Vollhardt D., *Phys. Rev. Lett.*, **115** (2015) 106402.
[28] Kubo R., *J. Phys. Soc. Jpn.*, **12** (1957) 570.
[29] Stinchcombe R. B., *Kubo and Zubarev formulations of response theory,* in *Nato Advanced Study Institute Series, Series B: Physics*, Vol. **35** (Plenum Press) 1978.
[30] Zubarev D. N., *Sov. Phys. Usp.*, **3** (1960) 320.
[31] Mahan G., *Many-Particle Physics*, third edition (Kluwer Academic/Plenum Publisher, New York) 2000.
[32] Yu P. Y. and Cardona M., *Fundamentals of Semiconductors* (Springer-Verlag, Berlin) 1999.
[33] Chadi D. J. and Cohen M. L., *Phys. Rev. B*, **8** (1973) 5747.
[34] Cunningham S. L., *Phys. Rev. B*, **10** (1974) 4988.
[35] Smith R. A., *Semiconductors* (Cambridge University, Cambridge England) 1978.
[36] Singleton J., *Band Theory and Electronic Properties of Solids, Oxford Master Series in Condensed Matter Physics*, 1st edition reprinted (Oxford University Press) 2010.
[37] Khasanov R. *et al.*, *New J. Phys.*, **12** (2010) 073024.
[38] McQueen T. M. *et al.*, *Phys. Rev. Lett.*, **103** (2009) 057002.
[39] Nakayama K. *et al.*, *Phys. Rev. Lett.*, **113** (2014) 237001.